Biosensors and Bioelectronics 145 (2019) 111715

Contents lists available at ScienceDirect

Biosensors and Bioelectronics

journal homepage: www.elsevier.com/locate/bios

# Single-step functionalization of poly-catecholamine nanofilms for ultra-sensitive immunosensing of ubiquitin carboxyl terminal hydrolase-L1 (UCHL-1) in spinal cord injury


Sultan Khetani[a,c], Vinayaraj Ozhukil Kollath[e], Erin Eastick[a,c], Chantel Debert[f,g], Arindom Sen[b,c,d,e], Kunal Karan[e], Amir Sanati-Nezhad[a,b,c,*]

[a] BioMEMS and Bioinspired Microfluidic Laboratory, Department of Mechanical and Manufacturing Engineering, University of Calgary, Calgary, Alberta, T2N 1N4, Canada
[b] Center for Bioengineering Research and Education, Schulich School of Engineering, University of Calgary, Calgary, Alberta, T2N 1N4, Canada
[c] Biomedical Engineering Graduate Program, University of Calgary, Calgary, Alberta, T2N 1N4, Canada
[d] Pharmaceutical Production Research Facility, Schulich School of Engineering, University of Calgary, Alberta, T2N 1N4, Canada
[e] Department of Chemical and Petroleum Engineering, University of Calgary, Calgary, Alberta, T2N 1N4, Canada
[f] Department of Clinical Neurosciences, Hotchkiss Brain Institute, Alberta Children Hospital Research Institute for Child and Maternal Health, University of Calgary, Calgary, Alberta, T2N 1N4, Canada
[g] Department of Clinical Neurosciences, Division of Physical Medicine and Rehabilitation, Foothills Medical Centre, University of Calgary, Calgary, Alberta, T2N 1N4, Canada

ARTICLE INFO

*Keywords:*
Polydopamine (pDA)
Poly-norepinephrine (pNE)
Spinal cord injury
Ubiquitin carboxyl terminal hydrolase (UCHL-1)
Immunosensor

ABSTRACT

Rapid, selective, and ultra-sensitive detection of brain and spinal cord injury markers in bodily fluids is an unmet clinical need. In this work, Polycatecholamine as a rich source of amine moieties was used for single-step fabrication of ultrasensitive immunosensors for the detection of Ubiquitin carboxyl-terminal hydrolase (UCHL-1) biomarker of brain and spinal cord injuries and address the clinical need. The surface of graphene electrodes was modified by electropolymerizing aqueous solution of dopamine (DA) and norepinephrine (NE) monomers for generating polycatecholamines nanofilms on the surface of graphene screen printed electrodes (GSPE) in a single functionalization step. Amine moieties of the polymer allowed immobilization of UCHL-1 antibody on the electrode. The single-step modification of GSPE offered a simple, ultrasensitive, and stable production of immunosensors for the detection of UCHL-1. The operational range of the UCHL-1 immunosensor developed with Polynorepinephrine pNE-modified is $0.1\,pg\,mL^{-1}$ – $10^5\,pg\,mL^{-1}$ (LOD: $1.91\,pg\,mL^{-1}$), and $1\,pg\,mL^{-1}$ – $10^5\,pg\,mL^{-1}$ (LOD: $0.70\,pg\,mL^{-1}$) with Polydopamine (pDA) modification, satisfying the clinical range. Both pNE and pDA modified immunosensors, detected UCHL-1 spiked in phosphate buffer saline, artificial cerebrospinal fluid, and serum. Along with the sensitive detections, selective performances were recorded in the above matrices in the presence of interfering neurotransmitters GABA and Glutamate as well as glial fibrillary acidic protein (GFAP). Upon testing clinical samples of spinal cord injury patients and healthy controls, both pNE and pDA immunosensors, delivered a comparable response for UCHL-1, thereby, making immunosensors useful for clinical settings.

## 1. Introduction

Ubiquitin carboxy-terminal hydrolase L1 (UCHL-1) is a deubiquitinating enzyme (Reyes-Turcu et al., 2009), responsible for degrading and eliminating misfolded proteins produced in cells (Orlowski, 1999). Expression of UCHL-1 is specific to neurons and neuroendocrine system accounting up to 2% of total brain proteins and in gonads (Doran et al., 1983; Liu et al., 2002). The dysfunction of UCHL-1 has been correlated to the severity of brain and spinal cord injuries, thereby providing a quantifiable marker to assess patients affected by these medical conditions (Adrian et al., 2016; Brophy et al., 2011; Yokobori et al., 2015). It is reported that the concentration of UCHL-1 peaks within 8 h post-traumatic brain injury and may be altered following seizures and other neurological conditions (Berger et al., 2012; Choi et al., 2004; Mondello

*Abbreviations:* pg, picogram; ng, nanogram; mL, millilitre; min, minutes; μL, microliter; LOD, limit of detection; SI, Supplementary Information

* Corresponding author. Department of Mechanical and Manufacturing Engineering, 2500 University Drive NW, Calgary, Alberta T2N 1N4, Canada.
*E-mail address:* amir.sanatinezhad@ucalgary.ca (A. Sanati-Nezhad).

https://doi.org/10.1016/j.bios.2019.111715
Received 9 August 2019; Received in revised form 17 September 2019; Accepted 17 September 2019
Available online 21 September 2019
0956-5663/ 

et al., 2012b). In the murine spinal cord injury model, the concentration of UCHL-1 in serum has been found to increase from 26.2 ng $mL^{-1}$ after 4 h post-injury to 4.58 ng $mL^{-1}$ after 24 h, and 2.63 ng $mL^{-1}$ after 7 days (Yang et al., 2018). In humans, UCHL-1 concentration in the serum reportedly increases from $1.2 \times 10^2$ pg $mL^{-1}$ for healthy controls to $2.35 \times 10^3$ pg $mL^{-1}$ after traumatic brain injury (TBI). Concentrations above $5.32 \times 10^3$ pg $mL^{-1}$ following the TBI can be fatal (Mondello et al., 2012a). There is still no human clinical data related to the concentration of UCHL-1 post-injury in spinal cord injury (SCI) patients.

Quantification of UCHL-1 is predominantly performed with western blotting and immunohistochemistry (North et al., 2012; Xiang et al., 2012). Enzyme-linked immunosorbent assay (ELISA) is used for detecting UCHL-1 in bodily fluids, including serum (Aswani Kumar et al., 2018; Lequin, 2005; Singh et al., 2018; Zhou et al., 2018). However, these time-consuming, multistep techniques are not suitable for point of care detection or frequent monitoring central nervous system (CNS) injury. On the other hand, electrochemical immunosensors exhibit higher sensitivity and significantly lower detection limits compared to conventional detection tools (Feng et al., 2017; Guohua et al., 2017; Hui and Ying, 2017; Hui et al., 2016; Kim et al., 2018; Ricci et al., 2012; Salahandish et al. 2018b, 2019b; Talan et al., 2018; Xiaohong et al., 2017). Immunosensors can be generated by creating nanocomposites made from conductive materials (eg. silver, gold), and non-conductive functional materials (e.g. polyethyleneimine (PEI)) which are then functionalized in a multistep process to generate binding sites for antibodies on the substrate (Safavieh et al. 2016, 2017; Salahandish et al. 2018a, 2019a).

Among all conducting materials, graphene has gained popularity for the production of immunosensors, owing to its high conductivity and high carrier-density dependent electromobility, which are both crucial for electrochemical sensing (Bolotin et al., 2008; Du et al., 2008; Lee et al., 2008). However, the process of creating and functionalizing nanocomposites electrodes and turning them into immunosensors still remains a challenge(Khetani et al., 2018). Whereas multistep electrode modifications have resulted in the sensitivity required for the effective detection of low concentration markers (Gorodkiewicz et al., 2011; Khetani et al. 2017a, 2017b, 2018; Reeves et al., 2017), these functionalization protocols are difficult to scale up for clinical applications. Therefore, there is a need for a simple and effective electrode modification technique without sacrificing the sensitivity of the sensor.

Adhesive proteins in marine animals and mussels' inspired catecholamine polymers, polydopamine (pDA) and polynorepinephrine (pNE) modified surfaces have been extensively used for various biological applications such as molecular imprinting, creating biocompatible coatings, cell and tissue culture, cell sensing, and making hybrid hydrogels (Kajisa et al., 2018; Lee et al., 2007; Valente et al., 2017; Vedadghavami et al., 2017). In addition, catechol functional groups are known to bind with the carboxylic group of antibodies, resulting in nucleophilic reaction or Schiff base reaction between the antibody and the catechol modified surface (Lee et al., 2009). Therefore, in this work, we used pNE and pDA to modify the electrode surfaces and immobilize UCHL-1 antibody for detecting UCHL-1.

The interactions between UCHL-1 antibody and UCHL-1 antigen were measured through Square wave voltammetry (SWV) in the presence of 5.0 mM K $[Fe(CN)_6]^{3/4}$ redox probe. The single-step modification enabled the detection of UCHL-1 in phosphate-buffered saline (PBS), artificial cerebrospinal fluid (aCSF) and human blood serum between the range of $10^{-1}$ pg $mL^{-1}$ – $10^5$ pg $mL^{-1}$ on pNE immunosensor and 1 pg $mL^{-1}$ – $10^5$ pg $mL^{-1}$ on pDA immunosensor. The performances of the immunosensors were then successfully validated against ELISA and tested for detection of UCHL-1 in the blood of SCI patients.

## 2. Methods

### 2.1. Immunosensor development

Separate solutions of Norepinephrine (NE) and Dopamine (DA) were prepared individually by mixing 0.5, 1.0, 2.0 and 5.0 mg $mL^{-1}$ concentration of norepinephrine hydrochloride and dopamine hydrochloride with 50 mM tris buffer (pH 8.5). Tris buffer was prepared by mixing Tris-base in DI and adjusting the pH to 8.5 using a pH meter. Polymer precursors and the tris-buffer were then mixed and stirred for 15 min at 60 °C. Details of consumables, materials, and instruments used in this research are given in section SI.

By adding 100 µL of each of the precursors individually on separate graphene screen-printed electrodes (GSPEs) and applying cyclic voltammograms (CV) in the range of −0.8 V–0.8 V, at 100 $mVs^{-1}$ scan rates, NE and DA were electropolymerized into pNE and pDA, respectively. All pNE modified electrodes were modified by applying 15 CV cycles in the presence of NE solution, and pDA electrodes were modified by applying 14 CV cycles in the presence of DA solution. Details of the cycles selection are given in the result section describing the optimization of the CV cycles. Following electropolymerization, GSPEs were rinsed with deionized (DI) water to clean any residual precursor from the electrode's surface. The modified electrodes were then incubated with 50 µL of 50 µg $mL^{-1}$ UCHL-1 antibody diluted in PBS at 4 °C for 60 min. Following the incubation with the antibody, the electrodes were cleaned with PBS, and a blocking step was implemented. To prevent unspecific binding, the electrodes were incubated with 100 µL of 1% Bovine serum albumin (BSA) for 45 min at room temperature. BSA solution was prepared by dissolving solid BSA in PBS, mixing and stirring it with a magnetic stirrer, and filtering it with 0.2 µm filter. Finally, UCHL-1 immunosensors were rinsed with 200 µL of PBS and incubated again for 30 min at room temperature after adding 50 µL of samples with UCHL-1 spiked in three different test media. All the measurements were repeated three times unless otherwise specified. A schematic depiction of the steps required to create and work with the immunosensor is shown in Fig. 1.

### 2.2. Electrochemical measurements

Square wave voltammetry was used for all the electrochemical characterizations and detection of UCHL-1 on both the immunosensors. All the concentrations were tested in triplicates unless explicitly stated, and all the measurements were performed with 5.0 mM K $[Fe(CN)_6]^{3/-4}$ redox probes. SWV was optimized and set to an initial potential of −0.5 V (vs SCE), the final potential of 0.8 V, pulse height of 25 mV, step height 10 mV, and pulse width of 50 ms. All the electrochemistry data was processed, baseline corrected, and graphed with Origin Pro 2016 (OriginLab Corporation, USA).

### 2.3. Preparation of aCSF and the separation of serum from blood

Blood from healthy donors and SCI patients was secured using ethics #REB15-2138. BD Vacutainer serum separation tubes were used for separating serum from the whole blood. by following the protocol described earlier (Khetani et al., 2017a). Artificial cerebrospinal fluid was prepared using a protocol described in our previous work (Khetani et al., 2018).

### 2.4. Vibrational spectroscopy for electrode surface modification

Confirmation of the electrode surface modification with polycatecholamines was performed on an attenuated total reflectance (ATR)-Fourier transform Infrared (ATR-FTIR) spectroscope. The FTIR spectra of unmodified, pDA and pNE modified electrode surfaces were acquired in attenuated total reflectance (ATR) mode by placing the electrode onto the Germanium crystal of the spectroscope (Kollath

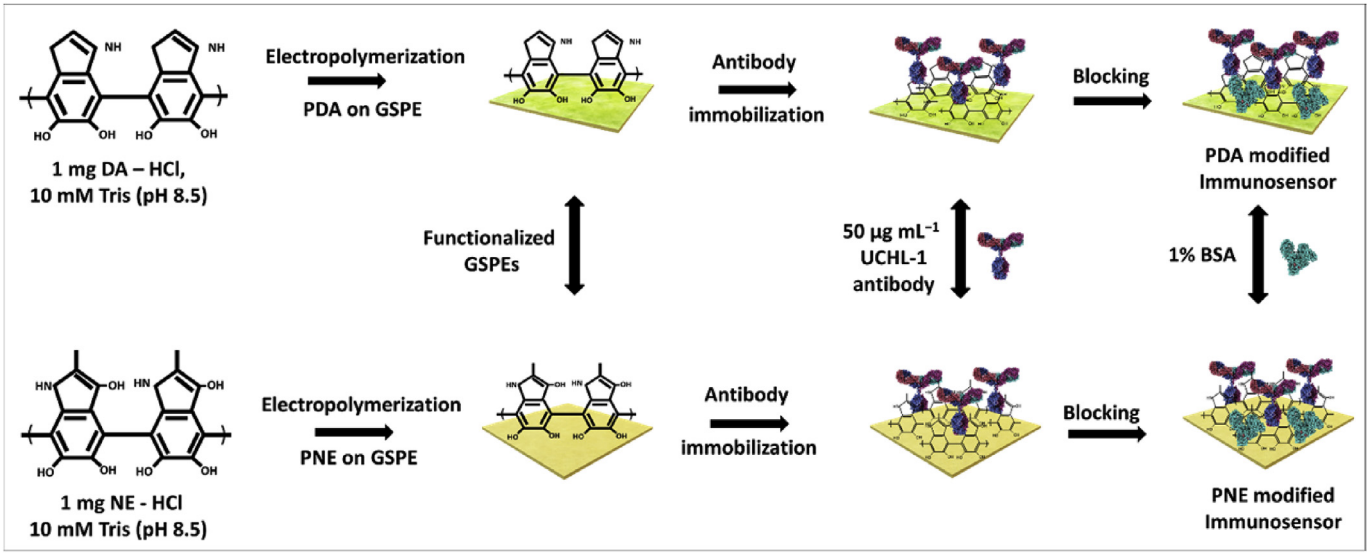


**Fig. 1.** A schematic representation of screen-printed electrode (SPE) modification steps required to generate the immunosensors for the detection of Ubiquitin carboxy-terminal hydrolase L1 (UCHL-1) detection. Monomers solution of 1 mg mL$^{-1}$ norepinephrine (NE) and 1 mg mL$^{-1}$ dopamine (DA) were prepared individually in 50 mM tris buffer (pH 8.5). By applying cyclic voltammetry, monomers were converted to respective polymers, polynorepinephrine (pNE) and polydopamine (pDA). Polycatecholamine modified electrodes were then immobilized with 50 µL of 50 µg mL$^{-1}$ UCHL-1 antibody followed by blocking the antibody free sites on the electrodes with 100 µL 1% bovine serum albumin (BSA). The marked the end of the immunosensor preparation steps, and they are now ready for detecting UCHL-1 from bodily fluids and media.

et al., 2016). The crystal was cleaned before every measurement, and a background spectrum of the surroundings was recorded for every sample tested at room temperature. ATR-FTIR spectra were recorded by averaging 32 scans at 4 cm$^{-1}$ between 4000 and 600 cm$^{-1}$ wavenumbers using a mid-IR KBr-DTGS detector.

### 2.5. Characterization of surface morphology

Morphology of the electrode surface was imaged using acoustic mode atomic force microscopy (AFM) using $Si_3N_4$ cantilever, and the images were analyzed with WSxM 5.0 software. In this mode, the electrode surface topography was recorded without any contact between the cantilever and the surface. The cantilever was subject to sinusoidal vibration of the frequency close to 132 kHz which is the cantilever's resonance frequency. The surface topography was recorded with 256 points/line at a scan rate of 0.4 line/s when the resonance amplitude of the cantilever is damped by 10% near the surface.

### 2.6. Measurement of polycatecholamine film thickness

The thickness of the polycatecholamine films formed on the surface of an electrode was determined by ellipsometric analysis. GSPEs have non-reflective surfaces, made on a ceramic substrate and laminated with plastic. Therefore, Si wafer was used as a model substrate for measuring the film thickness. The thickness of both polycatecholamine films was determined by drop-casting the pNE and pDA prepared by adding precursors individually to Tris-buffer and stirred it for 15 min at 60 °C on Si wafer. The thickness of the polymer thus formed on the Si was measured using an ellipsometer (model M2000U, J.A. Woollam Co., Inc.), and the data was analyzed with WVASE32 software. The wavelength of incident light ranged between 200 and 1000 nm, and the angles of incidence were selected to be 55°, 65°, and 75°. The thickness of the film on the Si substrate was calculated by fitting the spectrum data using the Cauchy model approximating the dispersion of the refractive index, and the data was analyzed. Each concentration of the polymer deposited was measured three times. The average value of the thickness and the standard error of the between measurements are reported.

### 2.7. Response of polycatecholamine immunosensors versus ELISA

Enzyme-linked immunosorbent assay (ELISA) was prepared according to the instruction manual from the vendor. 50 µL of each of the seven standards solutions, 0 (negative), 0.3125 ng mL$^{-1}$, 0.625 ng mL$^{-1}$, 1.25 ng mL$^{-1}$, 2.5 ng mL$^{-1}$, 5 ng mL$^{-1}$, 10 ng mL$^{-1}$and 20 ng mL$^{-1}$, prepared by serial dilution of the stock, were added to the plate. 50 µL of 0.6 ng mL$^{-1}$, 0.8 ng mL$^{-1}$, 0.9 ng mL$^{-1}$, and 5 ng mL$^{-1}$ UCHL-1 concentrations spiked in PBS was added to separate wells in the ELISA plate. Samples were incubated for 60 min before washing them three times with 350 µL washing buffer. The cocktail antibody was added to each well and the plate incubated on a plate shaker at 400 rpm for 60 min at room temperature. After the incubation, each well with the antibody was again washed three times with 350 µL of washing buffer. In the final step, 100 µL of 3,3′,5,5′-Tetramethylbenzidine (TMB) solution was added to each well, and the plate was incubated on a plate shaker at 400 rpm for 10 min at room temperature. Following the incubation, the reaction was stopped by adding 100 µL of stop solution to each well and the plate was incubated for 1 min on the plate shaker for mixing the solution. The absorbance was then measured at 450 nm. Known concentrations of UCHL-1 (0.6 ng mL$^{-1}$,0.8 ng mL$^{-1}$, 0.9 ng mL$^{-1}$, and 5 ng mL$^{-1}$) were tested with ELISA and both the immunosensors to compare the performance of the two techniques. Absorbance was recorded for ELISA, and SWV responses were recorded as described in the electrochemical measurements section.

## 3. Results and discussion

### 3.1. Optimizing the precursor concentration

To find the optimum concentration of DA and NE for modifying the electrodes, 0.5 mg mL$^{-1}$, 1 mg mL$^{-1}$ 2 mg mL$^{-1}$ and 5 mg mL$^{-1}$ concentrations of both the precursors were electropolymerized on GSPEs. Film thicknesses on the Si surface increased with the increase in the concentration of the polymers. The thickness of the film varied from 1.43 nm for 0.5 mg mL$^{-1}$ to 2.38 nm for 5 mg mL$^{-1}$ for pNE coated Si wafers and 6.24 nm–8.68 nm for pNE coated Si wafers (Fig. S1. B).

Thus, the functionalized GSPEs have nanometer-sized film thickness on its surface.

To measure the electrical response of GSPE to different polymer concentrations, SWV was performed in the presence of the redox probe, and the peak current was determined. The peak current decreased with increasing catecholamine concentration on the surface due to the increase in the thickness of the polymer film of the electrode resulting in decreased diffusion of redox ion on the working electrode. The SWV peak current decreased from 340.48 μA for the blank electrode, remained nearly the same at 340.56 μA for 0.5 mg $mL^{-1}$, and then decreased to 338.35 μA for 1 mg $mL^{-1}$, 296.76 μA for 2 mg $mL^{-1}$ and 258.86 μA for 5 mg $mL^{-1}$ concentration of the pNE (Fig. S1. A). pDA functionalized electrode also showed decreasing peak current the decline was steeper compared to pNE (Fig. S1. B and Fig. S2). For pDA functionalized GSPEs, the SWV peak current decreased from 341.15 μA for the uncoated electrode to 259.16 μA for 0.5 mg $mL^{-1}$, 255.28 μA for 1 mg $mL^{-1}$, 238.268 μA for 2 mg $mL^{-1}$, and 198.07 μA for 5 mg $mL^{-1}$.

Although 1 mg $mL^{-1}$ of pNE and 2 mg $mL^{-1}$ of pDA are widely used concentrations in coating surfaces and sensing applications (Kajisa et al., 2018). SWV peaks clearly showed that 2 mg $mL^{-1}$ and 5 mg $mL^{-1}$ and concentrations create a highly resistive surface compared to the unmodified surface for both materials, which is not the desire of biosensing applications. As the thicknesses of the surface with 0.5 mg $mL^{-1}$ and 1 mg $mL^{-1}$ of pDA were statistically indifferent (Fig. S1), 1 mg $mL^{-1}$ of pDA was selected for creating immunosensors. For pNE, although there is not a significant difference between the thicknesses in 0.5 mg $mL^{-1}$ and 1 mg $mL^{-1}$, the SWV signal of 0.5 mg $mL^{-1}$ is the same as that of the unmodified electrode. It implied that 0.5 mg $mL^{-1}$ did not create enough binding sites. Therefore, 1 mg $mL^{-1}$ of pNE was chosen for creating immunosensors.

Electroactive area of the modified electrodes was estimated using the Randles–Sevcik Equation, known as $i_p = kACD^{1/2}n^{3/2}v^{1/2}$ (Strømme et al., 1995), where, $i_p$ is peak of the redox current, $K = 2.68 \times 10^5$ is the experimental coefficient, $A$ is electroactive area in $cm^2$, $D = 6.7 \times 10^{-6}$ diffusion coefficient of the redox ferricyanide in $cm^2$ $s^{-1}$, $n$ is number of electrons transferred in the redox reaction (in this case $n = 1$), $v = 0.1$ *is* scan rate in V/s (100 $mVs^{-1}$), and $C = 5 \times 10^{-3}$ is concentration of the redox probes in mol $L^{-1}$ (5 mM $mL^{-1}$). For the polycatecholamines modified GSPE, the electroactive area decreased by 4% for pNE and 7.43% for pDA. It reduced from 362 $mm^2$ for the unmodified electrode to 347 $mm^2$ and 335 $mm^2$ for the pNE and pDA, respectively.

### 3.2. Optimization of the CV cycles and fourier-transform infrared spectroscopy (FTIR) characterization

The oxidative polymerization results in DA oxidizing to dopamine quinone, followed by cyclisation to form leucodopmainechrome (Barclay et al., 2017; Dreyer et al., 2012). This was followed by dopaminechrome, isomerizing to generate 5,6-dihydroxy-indole, where it finally oxidized to form the polymer. Thus, the peak anodic current was used to indicate the functionalization of the electrodes with pNE and pDA. To identify the number of scans required for the electropolymerization of both the polymer precursor, CV with different scan numbers applied to the electrodes until the peak anodic current remains unchanged.

With the increase in the cycles, the peak anodic current deceased until the 15th CV cycle for pNE and 14th CV cycles for pDA treated electrodes. After this, the peak anodic current began to overlap, indicating the completion of the electrode's surface modification with the polymers. Therefore, 15 CV scans were selected as the optimum scan number for oxidizing NE to pNE and DA to pDA on GSPEs (Fig. S3 A, B).

The confirmation of the GSPE's surface modification, ATR-FTIR was performed on the unmodified and modified electrodes. Spectra of unmodified and polycatecholamines-modified electrodes are shown in Fig. 2A. The unmodified GSPE showed only the significant peaks of the substrate carbon at 1348 $cm^{-1}$ 1456 $cm^{-1}$ (Kollath and Karan, 2016). As both the pDA and pNE are nearly similar materials, dihydroxy indole group in the polymerized forms is expected to be formed on the modified electrodes (Hong et al., 2013; Lee et al., 2007). The two major absorbance bands in 3000–2800 $cm^{-1}$ represent the symmetric and asymmetric CH stretching from the aliphatic chains present. The structure of pDA and pNE is a supramolecular arrangement consisting of charge transfer, pi-stacking, and hydrogen bonding interactions consisting of 5,6-dihydroxyindoline and its dione derivative (Barclay et al., 2017; Dreyer et al., 2012; Lee et al., 2007). The spectra of pDA and pNE in the signature region 1700 $cm^{-1}$ – 600 $cm^{-1}$ showed the known peaks associated with the C–C stretching and deformation modes (1284, 1035, 1503, 1625,2847, 2916 $cm^1$) from Indoline compound (Sullivan and Meyer, 1984). Thus, FTIR characterization confirmed the electrodeposition of both pDA and pNE and selection of CV scans for modifying the GSPE.

### 3.3. Diffusion kinetics

To assess the diffusion mechanism of the redox probe at the surface of the immunosensor, CV of scan rates varying from 10 mV $s^{-1}$ to 100 $mVs^{-1}$ was applied. Cathodic current peak (Ipc) and anodic current peak (Ipa) from CVs increased with the increase in the square root of scan rate for both the modified surfaces. A linear relationship was observed between Ipc ($R^2 = 0.98$) and Ipa ($R^2 = 0.99$) for the pNE modified GSPEs, and the Ipc ($R^2 = 0.92$) and Ipa ($R^2 = 0.96$) for the pDA modified GSPEs (Fig. S4). The discrete change in the current peaks compared with the unmodified GSPEs proves the occurrence of reversible and diffusion controlled electrochemical reactions on the electrode surface.

### 3.4. Atomic force microscopy of modified electrodes

AFM was used in the acoustic mode for imaging the surface modifications of the electrodes (Fig. 2). Uncoated GSPE showed several layers of graphene sheets with sharp edges, and root mean squared (RMS) roughness of 33 nm, and 92 nm (Fig. 2 B, E). After the electropolymerizing of electrodes, thin-film commonly associated with pNE surface, and agglomerates typical with pDA were observed in AFM images of the electrodes (Fig. 2 C, F). The roughness of the electrode surface also changed after the modification and increased to 53 and 111 nm respectively for the pNE and pDA modified surfaces. Following the immobilization of UCHL-1 antibody on both electrodes, globular morphology due to antibody appears on the electrode surface (Fig. 2 D, G). The values of RMS roughness reduced to 31 nm and 41 nm for pNE and pDA electrodes, respectively, indicating successful adsorption of UCHL-1 antibody on the modified electrode surfaces.

### 3.5. Electrochemical characterization of UCHL-1 immunosensors

The unmodified GSPE offered the highest conductivity in the presence of redox probes in comparison with the modified electrodes. However, the SWV peak current peaks decreased after the polymerization of pDA and pNE due to the non-conducting nature of their films. As the antibody, blocking agent BSA and UCHL-1 are also non-conductive, the peak current for both the immunosensors showed a decreasing trend (Fig. 3). The peak current for the pNE modified immunosensor decreased from 338.35 μA–309.72 μA after the immobilization of the antibody, then to 205.79 μA for BSA, and, finally to 185.76 μA for $10^{-1}$ pg $mL^{-1}$ of UCHL-1 (Fig. 3A).

pDA modified immunosensors also showed a decreasing trend of the peak currents by registering a drop of 85.2 μA. The peak current in the pDA modified immunosensor decreased from 255.29 μA after the pDA modification to 234.36 μA after the immobilization of the antibody, then to 149.76 μA for BSA, and finally to 132.54 μA for 1 pg $mL^{-1}$ of UCHL-1 (Fig. 3B). The immobilization of the anti-UCHL-1 antibody

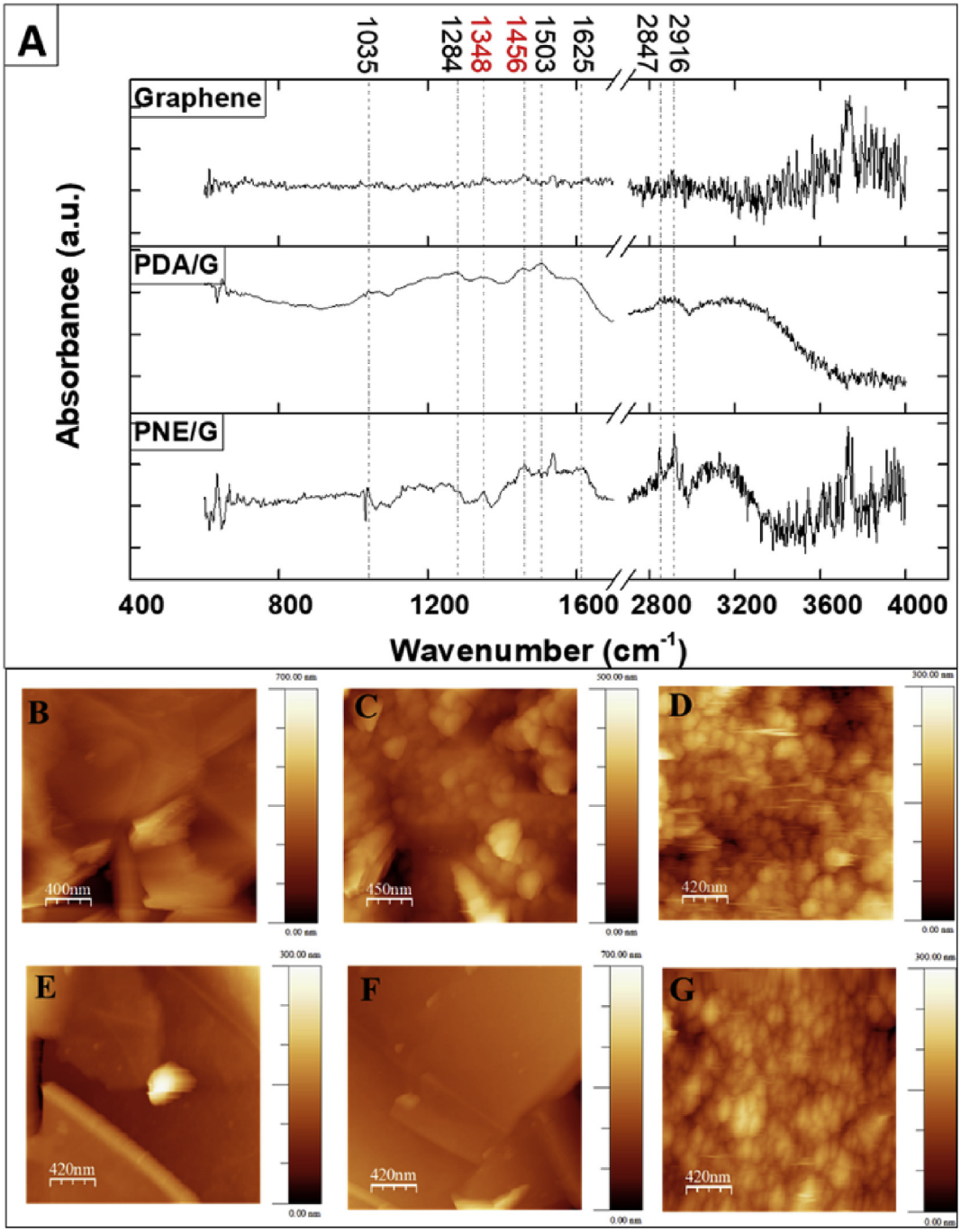


**Fig. 2.** Confirmation of the surface modification on the electrode characterized using Fourier transform Infrared spectroscopy (FTIR) and Atomic force microscopy (AFM). (**A**) attenuated total reflectance (ATR)-FTIR spectra of the unmodified GSPE, pDA modified Graphene and pNE modified graphene surface. AFM images, in acoustic mode for (**B, E**) Unmodified graphene working electrode, (**C**) pDA graphene electrode (**D, G**) Polycatecholamines modified electrodes with UCHL-1 antibody adsorbed. (**F**) pNE modified graphene electrode.

resulted in a decrease in the current peak due to the steric hindrance effect from the non-conducting antibody. After the addition of 1% BSA due to the non-conducting nature of the protein, the peak current decreased further, confirming the adsorption of BSA onto the modified GSPEs. Although the SWV peak currents decreased for both the electrodes, pNE modified electrodes were found to be more conductive in comparison with pDA modified electrodes. The higher conductivity of pNE compared to pDA is owed to the thinner film and polymeric structure(s).

### *3.6. Analytic range and limit of detection (LOD)*

For determining the analytical range of operation, UCHL-1 antigen samples with concentrations between $10^{6}$ pg mL$^{-1}$ - $10^{-2}$ pg mL$^{-1}$ were prepared in PBS as the base matrix (Fig. 3 C, D). On pNE modified immunosensors, concentrations between $10^{-2}$ pg mL$^{-1}$ and $10^{6}$ pg mL$^{-1}$ were tested while the pDA modified immunosensors were tested with $10^{-1}$ pg mL$^{-1}$ to $10^{6}$ pg mL$^{-1}$ concentrations. The SWV current peak for $10^{-2}$ pg mL$^{-1}$ concentration on pNE modified and $10^{-1}$ pg mL$^{-1}$ concentration on pDA modified immunosensor coincided with the baseline signal obtained after the addition of the

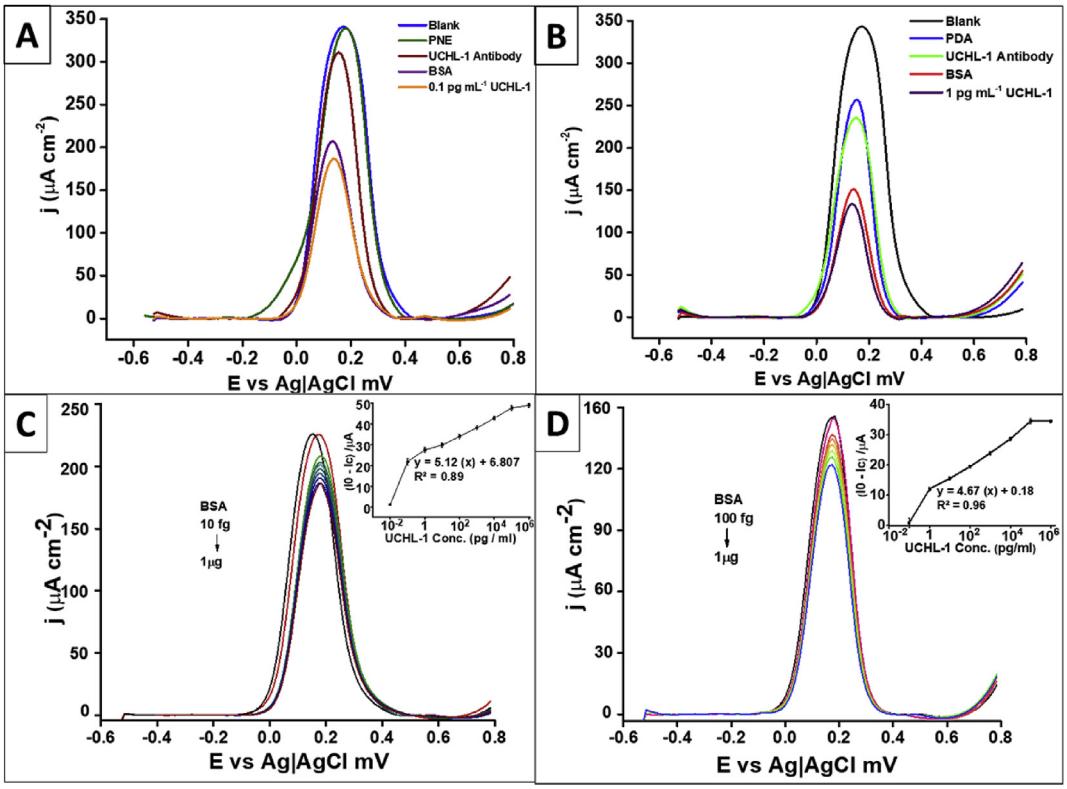


**Fig. 3.** Electrochemical characterization of the (**A**) pNE and (**B**) pDA modified immunosensors by measuring the SWV signals in the presence of redox probes. The signals are stacked in the order as follows: unmodified or the blank electrode, pNE or pDA modified electrodes, UCHL-1 antibody immobilized on the electrode surface, BSA blocked, and finally UCHL-1 antigens (n = 3). The linear detection range of pNE and pDA modified immunosensor, and their calibration curves are shown. The detection range is determined to be (**C**) $10^{-1}$ pg mL$^{-1}$ – $10^{5}$ pg mL$^{-1}$ for pNE modified immunosensor and (**D**) 1 pg mL$^{-1}$ – $10^{5}$ pg mL$^{-1}$ for pDA modified immunosensor (n = 3).

blocking agent (1% BSA). However, characteristic SWV current peaks were observed for the UCHL-1 concentration between $10^{-1}$ pg mL$^{-1}$ to $10^{5}$ pg mL$^{-1}$ for the pNE modified immunosensor, and between 1 pg mL$^{-1}$ to $10^{5}$ pg mL$^{-1}$ for the pDA modified immunosensor (Fig. 3 C, D). In both pDA and pNE modified immunosensors, the peak current saturation occurred for $10^{5}$ pg mL$^{-1}$ UCHL-1 concentration. Immunosensors would have reached the saturation point due to the insulating property of the antigen-antibody immunocomplex layer the formed on the electrode preventing further diffusion of the redox ions, unavailability of binding sites, diminished the competition for antigen to bind antibody on the immunosensor, and increased repulsive electrostatic interaction between $[Fe(CN)_6]^{-3/4}$ and the antibody-antigen complex (Huang et al., 2010).

By plotting the absolute peak current ($I_0$-$I_C$) (where $I_0$ is the SWV peak current after BSA and $I_C$ is the SWV peak current after the concentration tested) as a function of different concentrations tested. The equation for the correlation was determined to be y = 5.12 ($x$) + 6.81 (where ($x$) is the logarithmic concentration of UCHL-1 in pg mL$^{-1}$), with a coefficient of correlation ($R^2$) of 0.89 for the pNE modified immunosensor, and y = 4.67 ($x$) + 0.18 with $R^2$ of 0.96 for pDA modified immunosensors (inset Fig. 3 C, D).

Limit of detection (LOD) signifies the minimum concentration of UCHL-1 for which the SWV peak current for a concentration of UCHL-1 can be distinguished from the SWV peak current without the target UCHL-1. LOD is expressed as [(3* std. dev. of low conc.)/ slope of the calibration curve]. LOD was determined to be 1.91 pg mL$^{-1}$ for the pNE modified immunosensor and 0.7 pg mL$^{-1}$ for pDA modified immunosensor. The robust sensitivity of both pDA and pNE modified immunosensors can be attributed to the biocompatible properties of pDA and pNE, which both offer low background current and the sensitive SWV detection technique.

### 3.7. Detecting UCHL-1 in different matrix

The concentration range identified in the calibration curve for pNE ($10^{-1}$ pg mL$^{-1}$ - $10^{5}$ pg mL$^{-1}$) and pDA (1 pg mL$^{-1}$ - $10^{5}$ pg mL$^{-1}$) modified immunosensors, were prepared in human serum and aCSF. Samples in the matrices were tested in the presence of redox probes for SWV current peaks. The results show that the increase in the concentration resulted in a decrease in the SWV current peaks for samples prepared in serum and aCSF (Fig. S5). The absolute current and the UCHL-1 concentration were found to be linearly correlated as it is in the calibration curve with PBS (Fig. 4A and B).

For the UCHL-1 concentration range of $10^{-1}$ pg mL$^{-1}$ – $10^{5}$ pg mL$^{-1}$ tested on pNE immunosensor in aCSF and serum, the linear regression relationship between the absolute current and logarithm of the concentration of y = 4.38 ($x$) + 13.4 ($R^2$ = 0.97) with the LOD of 0.5 pg mL$^{-1}$, and y = 4.21 ($x$) + 15.16 ($R^2$ = 0.98) with the LOD of 1.68 pg mL$^{-1}$ were detected, respectively (Fig. 4A). Similarly, pDA modified immunosensor delivered equally reliable detection for the change in the base matrix when tested for the 1 pg mL$^{-1}$ – $10^{5}$ pg mL$^{-1}$concentration range. The linear regression relationship of y = 4.84 ($x$) + 17.02 ($R^2$ = 0.98) with the LOD of 0.63 pg mL$^{-1}$ and y = 5.7 ($x$) + 9.79 ($R^2$ = 0.99) and LOD of 0.85 pg mL$^{-1}$ was reported for detecting UCHL-1 spiked in serum and aCSF, respectively (Fig. 4B). These tests proved the reliable performance for both polycatecholamines immunosensors for detecting target UCHL-1 in different matrices without any significant deviation in sensitivity, stability and detection range.

### 3.8. Selectivity of detection

Selectivity test was performed to identify if biomarkers such as

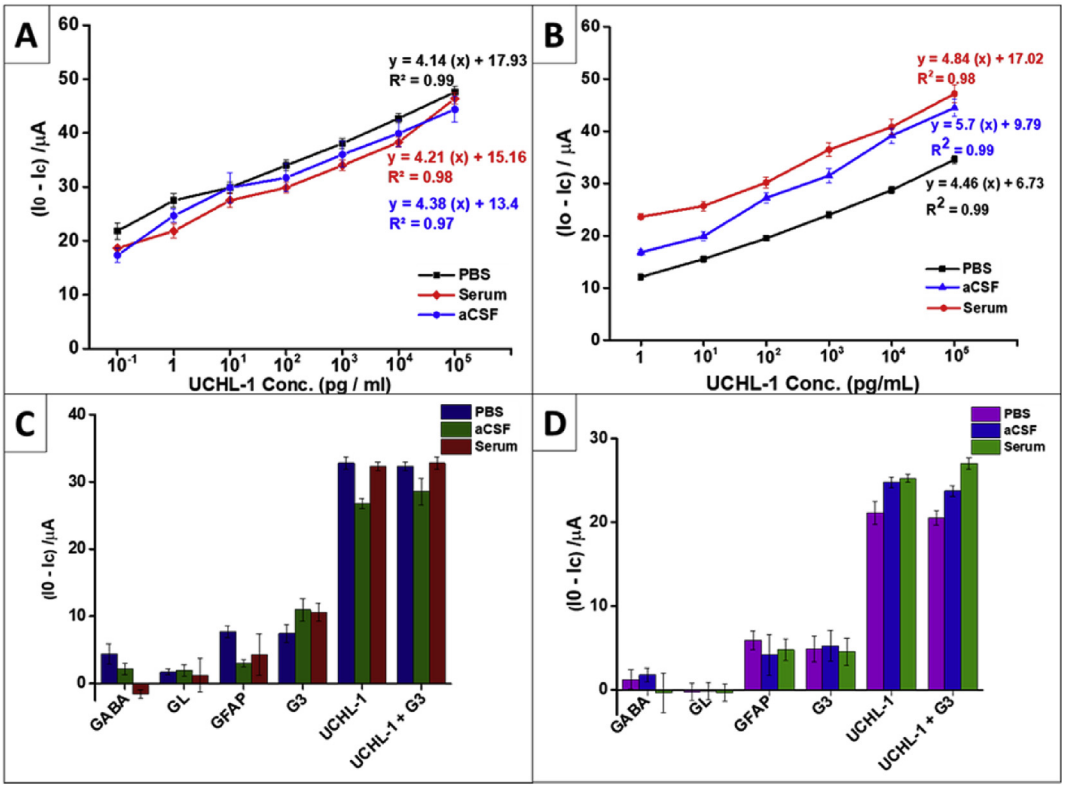


**Fig. 4.** Detection of UCHL-1 in different matrices and the selectivity response of the immunosensors. UCHL-1 detected in PBS, blood serum and aCSF were recorded for (**A**) pNE, (**B**) pDA modified immunosensors. Selectivity response of the UCHL-1 immunosensors was tested in the presence of the target and other interference markers by preparing samples in PBS, aCSF, and Serum. Immunosensors were tested with the following targets: GABA, GL (glutamate), GFAP (glial fibrillary acidic protein), G3 (GABA, GL, and GFAP), UCHL-1 + G3. The responses were recorded for (**C**) pNE and, (**D**) pDA modified immunosensors (n = 3).

Glutamate (GL), gamma-Aminobutyric acid (GABA), Glial fibrillary acidic protein (GFAP) interfere in the detection of UCHL-1. In each of the three matrices, GL, GABA, GFAP, and UCHL-1were each tested alone, as well as a cocktail of GL + GABA + GFAP (collectively called G3), and G3 + UCHL-1. The concentration of the potentially interfering biomarkers and UCHL-1 were selected based on their concentrations after the injury (Allen et al., 2004; North et al., 2012).

pNE immunosensors delivered a UCHL-1 signal of 32.80 µA in PBS, 26.79 µA in aCSF, and 32.33 µA in serum. When UCHL-1 was tested with the G3 biomarkers, UCHL-1 signal was well within the error margin at 32.34 µA for PBS, 28.54 µA for aCSF, and 32.80 µA for serum. Similarly, for pDA immunosensors, the UCHL-1 signal was 21.12 µA for PBS, 24.79 µA for aCSF, and 25.27 µA for serum, while the signal was 20.51for PBS, 23.74 µA for aCSF, 27.02 µA for serum when UCHL-1 was tested in the presence of G3 biomarkers. The highest absolute peak observed for the interfering biomarkers was 10.63 µA for the pNE modified immunosensor and 5.92 µA for the pDA modified immunosensor (Fig. 4 C, D). These total peak currents are significantly lower when compared with the absolute peaks current for the UCHL-1 and the UCHL-1 with the cocktail of the interfering biomarkers tested with both the immunosensors.

The selectivity test confirmed that the detection of the UCHL-1 in the presence of interfering biomarkers is almost three times higher for both pNE and pDA-modified immunosensors across the different matrices. This highly selective performance of the immunosensors is a direct result of the substrate property, the strong binding affinity between the UCHL-1 and the antibody on the immunosensors, and ability of the polycatecholamine-modified immunosensors to maintain a high aspect ratio of antigen-antibody binding on the sensor.

### 3.9. Reproducibility

Reproducibility was tested by preparing five different immunosensors with GSPE/pNE/anti-UCHL-1/antibody/BSA, and another five GSPE/pDA/anti-UCHL-1-antibody/BSA. The reproducibility response of pNE and pDA modified immunosensors was examined with the control concentration (0 pg $mL^{-1}$) and by testing $10^3$ pg $mL^{-1}$ UCHL-1 in PBS. The relative standard deviation (RSD) was calculated for measuring the precision of the signal with respect to the mean signal as 100 * S/ |X| where, S is the sample standard deviation and X is sample average. The measured peak currents on the pNE immunosensors were 229.79 µA (RSD of 1.02%) and 204.65 µA (RSD of 1.55%) for 0 pg $mL^{-1}$and$10^3$ pg $mL^{-1}$ UCHL-1 respectively. On the pDA modified immunosensors, 146.92 µA (RSD of 2.83%) and 129.95 µA (RSD of 2.62%) were recorded for 0 pg $mL^{-1}$ and $10^3$ pg $mL^{-1}$ UCHL-1 respectively. This demonstrates a consistent signal for the concentration tested, and a high signal difference compared with the control concentration.

### 3.10. Comparison with ELISA and clinical samples

Correlation between the performance of UCHL-1 ELISA and the immunosensors was established to validate and compare the performance of the immunosensors. UCHL-1 concentrations of 0.6 ng $mL^{-1}$, 0.8 ng $mL^{-1}$, 0.9 ng $mL^{-1}$, 5 ng $mL^{-1}$ concentrations were spiked in PBS and measured with both ELISA and electrochemically with the immunosensors (Fig. 5). Recovery (%) for ELISA and immunosensors was calculated as Recovery (%) = (Observed signal/ Expected signal) x 100.

The signal observed with pNE and pDA immunosensors and the signal expected based on correlations is documented in (Table S1). Highly comparable performance in terms of recovery of the

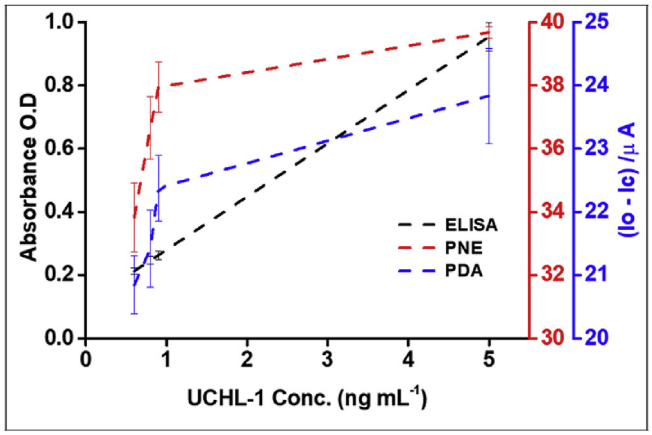


**Fig. 5.** Performance comparison between the response of ELISA (in black), pNE modified immunosensor (in red), and pDA modified immunosensors (in blue). All the three were tested with 0.6 ng mL$^{-1}$, 0.8 ng mL$^{-1}$, 0.9 ng mL$^{-1}$, 5 ng mL$^{-1}$ UCHL-1 spiked in PBS. Each data point represents three independent measuremnts (n = 3) and the error is standard error of the mean. (For interpretation of the references to colour in this figure legend, the reader is referred to the Web version of this article.)

**Table 1**
Detection of UCHL-1 from healthy and clinical SCI patients.

| Sample code | pNE electrode Detection (pg mL$^{-1}$) | pDA electrode Detection (pg mL$^{-1}$) |
|---|---|---|
| Control – C1 | 1.04 | 1.41 |
| Control – C2 | 0.61 | 1.37 |
| Control – C3 | 1.43 | 2.83 |
| SCI–S1 | 24.32 | 24.54 |
| SCI–S2 | 61,650 | 55,080 |
| SCI–S3 | 15.88 | 14.38 |

concentrations tested and low % RSD in the range of 2.34%–3.29% and 1.33%–5.22% were observed for pNE and pDA modified immunosensors, respectively. The polycatecholamine functionalized immunosensors delivered these results within 30 min, which was far quicker when compared to the ELISA assays, which took over 3 h to deliver similar results and required multiple rendering steps before detection.

The comparison test established the reliability of measuring samples with unknown concentration using immunosensors. Therefore, serum samples from three healthy control (Control - C1 to C3) and three SCI patients (SCI – S1 to S3) were tested for UCHL-1 using the developed immunosensors. The concentration of UCHL-1 was determined by feeding the absolute peak current value to the equation of the serum response of the immunosensors. In healthy controls, the concentration of UCHL-1 was close to the lower detection limit of both immunosensors, indicating no presence of the target. In the three clinical samples, UCHL-1 was found in varying concentrations as shown in Table 1.

The variation in the absolute concentration between the immunosensors can be attributed to the material used in functionalization and the matrix-dependent response of both the immunosensors. With these findings, it was evident that pDA and pNE modified immunosensors could be to reliably detect UCHL-1 in the serum of clinical samples.

The high analytic range of operation and the limit of detection of both polycatecholamine immunosensors are in agreement with previously reported electrochemical sensors developed with a pDA functionalized on the electrodes for the detection of antigen and several other targets (Table S2). The polycatecholamine functional material and the electrochemical detection technique improved the detection range and the LOD by three times compared with the UCHL-1 immunosensors reported earlier (Table S3).

## 4. Conclusion

In this study, we demonstrated electrochemical immunosensors developed by engineering biomimetic polycatecholamine nanofilms on a GSPE surface for the detection of UCHL-1. The immunosensors offered highly sensitive, wide linear detection range and LOD ($10^{-1}$ pg mL$^{-1}$ – $10^{5}$ pg mL$^{-1}$, 1.91 pg mL$^{-1}$) with pNE and (1 pg mL$^{-1}$ – $10^{5}$ pg mL$^{-1}$, 0.7 pg mL$^{-1}$) with pDA biopolymers used in functionalizing the GSPE. Both the immunosensors offered a high-performance range encompassing the physiologically relevant range of UCHL-1 because of the systematic characterization, and optimization of the concentration, graphene electrode and the SWV technique used of the detection.

This is the first report of electrochemical immunosensors with functionalized polycatecholamines capable of reproducibly detecting UCHL-1 at clinically relevant levels in human serum and aCSF. The sensors provided results 6 times faster than ELISA, the current gold standard used for clinical detection, and required fewer processing steps. Immunosensors developed by engineering biomimetic material and modifying GSPEs in a single step can be used diagnostically in resource-constrained setting for improving the care of patients' spinal cord and other CNS injuries.

## Associated content

### *Supporting information*

The supporting information is available free of charge on the BIOS publication website at DOI: 00.000./BIOS.0000.

Materials (chemical, reagents, and instruments), SWV of different polymer concentrations, thickness of the polymer films, current peaks v/s scan rates, SWV signals for UCHL-1 in aCSF and serum, calculation for comparing the performance of immunosensors with ELISA, electrochemical sensors developed with pDA, and comparison between the performances of different immunosensors developed for detecting UCHL-1 are listed in the supporting information file.

## Declaration of competing interest

The authors declare that they have no known competing financial interests or personal relationships that could have appeared to influence the work reported in this paper.

## Acknowledgements

The authors acknowledge Natural Sciences and Engineering Research of Canada (NSERC); Canada Research Chair; Alberta Prion Research Institute (APRI); Alberta Innovates BioSolutions (AIBS); and CMC – Microsystems, Canada for supporting this research.

## Appendix A. Supplementary data

Supplementary data to this article can be found online at https://doi.org/10.1016/j.bios.2019.111715.

## References

Adrian, H., Mårten, K., Salla, N., Lasse, V., 2016. Biomarkers of traumatic brain injury: temporal changes in body fluids. eNeuro 3 (6).
Allen, N.J., Káradóttir, R., Attwell, D., 2004. Reversal or reduction of glutamate and GABA transport in CNS pathology and therapy. Pflüg. Arch. 449 (2), 132–142.
Aswani Kumar, Y., Renuka, R., Achuth, J., Venkataramana, M., Ushakiranmayi, M., Sudhakar, P., 2018. Development of Hybrid IgG-Aptamer Sandwich Immunoassay Platform for Aflatoxin B1 Detection and its Evaluation onto Various Field Samples 9. Frontiers in pharmacology, pp. 271.

Barclay, T.G., Hegab, H.M., Clarke, S.R., Ginic-Markovic, M., 2017. Versatile surface modification using polydopamine and related polycatecholamines: chemistry, structure, and applications. Adv. Mater. Interfaces 4 (19), 1601192.
Berger, R.P., Hayes, R.L., Richichi, R., Beers, S.R., Wang, K.K., 2012. Serum concentrations of ubiquitin C-terminal hydrolase-L1 and αII-spectrin breakdown product 145 kDa correlate with outcome after pediatric TBI. J. Neurotrauma 29 (1), 162–167.
Bolotin, K.I., Sikes, K., Jiang, Z., Klima, M., Fudenberg, G., Hone, J., Kim, P., Stormer, H., 2008. Ultrahigh electron mobility in suspended graphene. Solid State Commun. 146 (9), 351–355.
Brophy, G.M., Mondello, S., Papa, L., Robicsek, S.A., Gabrielli, A., Tepas III, J., Buki, A., Robertson, C., Tortella, F.C., Hayes, R.L., 2011. Biokinetic analysis of ubiquitin C-terminal hydrolase-L1 (UCH-L1) in severe traumatic brain injury patient biofluids. J. Neurotrauma 28 (6), 861–870.
Choi, J., Levey, A.I., Weintraub, S.T., Rees, H.D., Gearing, M., Chin, L.-S., Li, L., 2004. Oxidative modifications and down-regulation of ubiquitin carboxyl-terminal hydrolase L1 associated with idiopathic Parkinson's and Alzheimer's diseases. J. Biol. Chem. 279 (13), 13256–13264.
Doran, J.F., Jackson, P., Kynoch, P.A., Thompson, R., 1983. Isolation of PGP 9.5, a new human neurone-specific protein detected by high-resolution two-dimensional electrophoresis. J. Neurochem. 40 (6), 1542–1547.
Dreyer, D.R., Miller, D.J., Freeman, B.D., Paul, D.R., Bielawski, C.W., 2012. Elucidating the structure of poly (dopamine). Langmuir 28 (15), 6428–6435.
Du, X., Skachko, I., Barker, A., Andrei, E.Y., 2008. Approaching ballistic transport in suspended graphene. Nat. Nanotechnol. 3 (8), 491–495.
Feng, H., Huang, Z., Lou, X., Li, J., Hui, G., 2017. Study of a Sucrose Sensor by Functional Cu Foam Material and its Applications in Commercial Beverages 10. Food analytical methods, pp. 407–418 2.
Gorodkiewicz, E., Ostrowska, H., Sankiewicz, A., 2011. SPR imaging biosensor for the 20S proteasome: sensor development and application to measurement of proteasomes in human blood plasma. Microchimica Acta 175 (1–2), 177–184.
Guohua, H., Hongyang, L., Zhiming, J., Danhua, Z., Haifang, W., 2017. Study of Small-Cell Lung Cancer Cell-Based Sensor and its Applications in Chemotherapy Effects Rapid Evaluation for Anticancer Drugs 97. Biosensors and Bioelectronics, pp. 184–195.
Hong, S., Kim, J., Na, Y.S., Park, J., Kim, S., Singha, K., Im, G.I., Han, D.K., Kim, W.J., Lee, H., 2013. Poly (norepinephrine): ultrasmooth material-independent surface chemistry and nanodepot for nitric oxide. Angew. Chem. Int. Ed. 52 (35), 9187–9191.
Huang, K.-J., Niu, D.-J., Xie, W.-Z., Wang, W., 2010. A disposable electrochemical immunosensor for carcinoembryonic antigen based on nano-Au/multi-walled carbon nanotubes–chitosans nanocomposite film modified glassy carbon electrode. Anal. Chim. Acta 659 (1–2), 102–108.
Hui, Guohua, Ying, Yibin, 2017. Quantitative rapid analysis method for ofloxacin in raw milk based on molecule-specific recognition and electrochemical impedance spectrum. Trans. ASABE 60 (5), 1439–1443.
Hui, G., Zhang, J., Li, J., Zheng, L., 2016. Sucrose Quantitative and Qualitative Analysis from Tastant Mixtures Based on Cu Foam Electrode and Stochastic Resonance 197. Food chemistry, pp. 1168–1176.
Kajisa, T., Yanagimoto, Y., Saito, A., Sakata, T., 2018. Biocompatible poly (catecholamine)-film electrode for potentiometric cell sensing. ACS Sens. 3 (2), 476–483.
Khetani, S., Aburashed, R., Singh, A., Sen, A., Sanati-Nezhad, A., 2017a. Immunosensing of S100β biomarker for diagnosis of spinal cord injuries (SCI). Sens. Actuators B Chem. 247, 163–169.
Khetani, S., Kundra, V., Sanati-Nezhad, A., 2017b. Synthesis of highly sensitive graphene nanocomposite for biosensing glial fibrillary acidic protein (GFAP). CMBES Proc. 40.
Khetani, S., Ozhukil Kollath, V., Kundra, V., Nguyen, M.D., Debert, C., Sen, A., Karan, K., Sanati-Nezhad, A., 2018. Polyethylenimine modified graphene-oxide electrochemical immunosensor for the detection of glial fibrillary acidic protein in central nervous system injury. ACS Sens. 3 (4), 844–851.
Kim, D., Kim, J.M., Jeon, Y., Lee, J., Oh, J., Antink, W.H., Kim, D., Piao, Y., 2018. Novel Two-step Activation of Biomass-Derived Carbon for Highly Sensitive Electrochemical Determination of Acetaminophen 259. Sensors and Actuators B: Chemical, pp. 50–58.
Kollath, V.O., Chen, Q., Mullens, S., Luyten, J., Traina, K., Boccaccini, A.R., Cloots, R., 2016. Electrophoretic deposition of hydroxyapatite and hydroxyapatite–alginate on rapid prototyped 3D Ti6Al4V scaffolds. J. Mater. Sci. 51 (5), 2338–2346.
Kollath, V.O., Karan, K., 2016. New molecular scale insights into the α-transition of Nafion® thin films from variable temperature ATR-FTIR spectroscopy. Phys. Chem. Chem. Phys. 18 (37), 26144–26150.
Lee, C., Wei, X., Kysar, J.W., Hone, J., 2008. Measurement of the elastic properties and intrinsic strength of monolayer graphene. Science 321 (5887), 385–388.
Lee, H., Dellatore, S.M., Miller, W.M., Messersmith, P.B., 2007. Mussel-inspired surface chemistry for multifunctional coatings. Science 318 (5849), 426–430.
Lee, H., Rho, J., Messersmith, P.B., 2009. Facile conjugation of biomolecules onto surfaces via mussel adhesive protein inspired coatings. Adv. Mater. 21 (4), 431–434.
Lequin, R.M., 2005. Enzyme immunoassay (EIA)/enzyme-linked immunosorbent assay (ELISA). Clin. Chem. 51 (12), 2415–2418.
Liu, Y., Fallon, L., Lashuel, H.A., Liu, Z., Lansbury Jr., P.T., 2002. The UCH-L1 gene encodes two opposing enzymatic activities that affect α-synuclein degradation and Parkinson's disease susceptibility. Cell 111 (2), 209–218.
Mondello, S., Akinyi, L., Buki, A., Robicsek, S., Gabrielli, A., Tepas, J., Papa, L., Brophy, G.M., Tortella, F., Hayes, R.L., 2012a. Clinical utility of serum levels of ubiquitin C-terminal hydrolase as a biomarker for severe traumatic brain injury. Neurosurgery 70 (3), 666.
Mondello, S., Palmio, J., Streeter, J., Hayes, R.L., Peltola, J., Jeromin, A., 2012b. Ubiquitin carboxy-terminal hydrolase L1 (UCH-L1) is increased in cerebrospinal fluid and plasma of patients after epileptic seizure. BMC Neurol. 12 (1), 85.
North, S.H., Shriver-Lake, L.C., Taitt, C.R., Ligler, F.S., 2012. Rapid analytical methods for on-site triage for traumatic brain injury. Annu. Rev. Anal. Chem. 5, 35–56.
Orlowski, R.Z., 1999. The role of the ubiquitin-proteasome pathway in apoptosis. Cell Death Differ. 6 (4), 303.
Reeves, J.P., Khetani, S., Sanati-Nezhad, A., 2017. Thin film silicon biosensor for the detection of spinal cord injury (SCI). CMBES Proc. 40.
Reyes-Turcu, F.E., Ventii, K.H., Wilkinson, K.D., 2009. Regulation and cellular roles of ubiquitin-specific deubiquitinating enzymes. Annu. Rev. Biochem. 78, 363–397.
Ricci, F., Adornetto, G., Palleschi, G., 2012. A review of experimental aspects of electrochemical immunosensors. Electrochim. Acta 84, 74–83.
Safavieh, M., Kaul, V., Khetani, S., Singh, A., Dhingra, K., Kanakasabapathy, M.K., Draz, M.S., Memic, A., Kuritzkes, D.R., Shafiee, H., 2017. Paper microchip with a graphene-modified silver nano-composite electrode for electrical sensing of microbial pathogens. Nanoscale 9 (5), 1852–1861.
Safavieh, M., Khetani, S., Juillard, F., Kaul, V., Kanakasabapathy, M.K., Kaye, K.M., Shafiee, H., 2016. Electrical response of a B lymphoma cell line latently infected with Kaposi's sarcoma herpesvirus. Biosens. Bioelectron. 80, 230–236.
Salahandish, R., Ghaffarinejad, A., Naghib, S.M., Majidzadeh-A, K., Zargartalebi, H., Sanati-Nezhad, A., 2018a. Nano-biosensor for highly sensitive detection of HER2 positive breast cancer. Biosens. Bioelectron. 117, 104–111.
Salahandish, R., Ghaffarinejad, A., Naghib, S.M., Niyazi, A., Majidzadeh-A, K., Janmaleki, M., Sanati-Nezhad, A., 2019a. Sandwich-structured nanoparticles-grafted functionalized graphene based 3D nanocomposites for high-performance biosensors to detect ascorbic acid biomolecule. Sci. Rep. 9 (1), 1226.
Salahandish, R., Ghaffarinejad, A., Omidinia, E., Zargartalebi, H., Majidzadeh-A, K., Naghib, S.M., Sanati-Nezhad, A., 2018b. Label-free ultrasensitive detection of breast cancer miRNA-21 biomarker employing electrochemical nano-genosensor based on sandwiched AgNPs in PANI and N-doped graphene. Biosens. Bioelectron. 120, 129–136.
Salahandish, R., Zargartalebi, H., Janmaleki, M., Khetani, S., Azarmanesh, M., Ashani, M.M., Aburashed, R., Vatani, M., Ghaffarinejad, A., Sanati-Nezhad, A., 2019. Reproducible and Scalable Generation of Multilayer Nanocomposite Constructs for Ultrasensitive Nanobiosensing. Advanced Materials Technologies 1900478.
Singh, S., Mishra, P., Banga, I., Parmar, A.S., Tripathi, P.P., Gandhi, S., 2018. Chemiluminescence based immunoassay for the detection of heroin and its metabolites. BioImpacts 8 (1), 53. https://doi.org/10.15171/bi.2018.07.
Strømme, M., Niklasson, G.A., Granqvist, C.G., 1995. Voltammetry on fractals. Solid State Commun. 96 (3), 151–154.
Sullivan, B.P., Meyer, T.J., 1984. Photoinduced irreversible insertion of CO 2 into a metal–hydride bond. J. Chem. Soc., Chem. Commun. (18), 1244–1245.
Talan, A., Mishra, A., Eremin, S.A., Narang, J., Kumar, A., Gandhi, S.J.B., Bioelectronics, 2018. Ultrasensitive Electrochemical Immuno-Sensing Platform Based on Gold Nanoparticles Triggering Chlorpyrifos Detection in Fruits and Vegetables, vol. 105. pp. 14–21.
Valente, K.P., Khetani, S., Kolahchi, A.R., Sanati-Nezhad, A., Suleman, A., Akbari, M., 2017. Microfluidic technologies for anticancer drug studies. Drug Discov. Today 22 (11), 1654–1670.
Vedadghavami, A., Minooei, F., Mohammadi, M.H., Khetani, S., Kolahchi, A.R., Mashayekhan, S., Sanati-Nezhad, A., 2017. Manufacturing of hydrogel biomaterials with controlled mechanical properties for tissue engineering applications. Acta Biomater. 62, 42–63.
Xiang, T., Li, L., Yin, X., Yuan, C., Tan, C., Su, X., Xiong, L., Putti, T.C., Oberst, M., Kelly, K., 2012. The ubiquitin peptidase UCHL1 induces G0/G1 cell cycle arrest and apoptosis through stabilizing p53 and is frequently silenced in breast cancer. PLoS One 7 (1), e29783.
Xiaohong, Z., Zhidong, Z., Xiongwei, L., Jian, L., Guohua, H., 2017. A Maltose, L-Rhamnose Sensor Based on Porous Cu Foam and Electrochemical Amperometric it Scanning Method 11. J. Food Measur. Charact., pp. 548–555 2.
Yang, Z., Bramlett, H.M., Moghieb, A., Yu, D., Wang, P., Lin, F., Bauer, C., Selig, T.M., Jaalouk, E., Weissman, A.S., 2018. Temporal profile and severity correlation of a panel of rat spinal cord injury protein biomarkers. Mol. Neurobiol. 55 (3), 2174–2184.
Yokobori, S., Zhang, Z., Moghieb, A., Mondello, S., Gajavelli, S., Dietrich, W.D., Bramlett, H., Hayes, R.L., Wang, M., Wang, K.K., 2015. Acute diagnostic biomarkers for spinal cord injury: review of the literature and preliminary research report. World Neurosurg. 83 (5), 867–878.
Zhou, Y., Wu, D., Hui, G., Mao, J., Liu, T., Zhou, W., Zhao, Y., Chen, Z., Chen, F., 2018. Loquat bruise detection using optical coherence tomography based on microstructural parameters. Food Analytical Methods 11 (10), 2692–2698.